Analytical Methods

PAPER

View Article Online
View Journal | View Issue

Cite this: *Anal. Methods*, 2016, **8**, 6847

Imaging of localized enzymatic peroxidase activity over unbiased individual gold nanowires by scanning electrochemical microscopy†‡

Preety Vatsyayan,[a] Christian Iffelsberger,[a] Carmen C. Mayorga-Martinez[b] and Frank-Michael Matysik*[a]

Received 1st July 2016
Accepted 15th August 2016

DOI: 10.1039/c6ay01875k

www.rsc.org/methods

Scanning electrochemical microscopy (SECM) in the constant-height mode was used to image individual gold nanowires (AuNWs, 2–3 μm long and ~140 nm diameter). High-resolution negative and positive feedback current images of individual AuNWs immobilized on glass and gold-coated glass slides, respectively, were recorded with a Wollaston-based platinum disk ultramicroelectrode (UME) of radius 300 nm at 0.3 V probe potential using ferrocenemethanol as the mediator. The negative and positive feedback current responses were dependent on the effective recycling of the mediator on the unbiased AuNWs. Furthermore, the AuNWs were covalently linked to horseradish peroxidase (HRP) and immobilized on a thin film gold substrate. Positive feedback and localized HRP activity over individual AuNWs were imaged subsequently by switching the probe potential from 0.3 V to 0 V after the addition of H_2O_2. In this measurement, ferrocenemethanol behaved both as the mediator (feedback response at 0.3 V probe potential) and the electron donor for HRP (in the presence of H_2O_2 for activity imaging at 0 V).

1. Introduction

Scanning electrochemical microscopy (SECM) is known to be a powerful tool for the investigation and imaging of the topography and surface reactivity of microstructured substrates.[1,2] It is a non-contact scanning probe imaging technique that has evolved from a low resolution electrochemical imaging system, after its introduction by Bard *et al.* in 1989, to a high resolution topographic imaging technique in recent years.[3,4] Recently, SECM has been used for imaging both living cells and non-living substrates with nanoscale resolution. However, the imaging at the nanoscale is largely dependent on the size of the probes. Lately, with the development of methods for the fabrication of sub-micrometer and nanometer sized probes for SECM, high-resolution topographic imaging has frequently been possible. The fabrication of SECM probes by pulling annealed Pt wires into capillaries through a laser puller enables the fabrication of probes with diameters as small as 50 nm with very small RG values (ratio of glass sheath radius to probe electrode radius). Such probes can be used to image living cells and non-living substrates with lateral resolutions as high as 100–200 nm.[5,6] However, the frequent use of such nanoprobes is still limited for many applications because of the difficulty in their handling and operation.

Besides providing topographic details, a very interesting aspect of SECM is the ability to study surface reactivity. This feature gives SECM an advantage over other microscopy techniques such as atomic force microscopy (AFM), scanning and transmission electron microscopy (SEM and TEM), *etc.*, which cannot provide information about the chemical reactivity of the surface. Thus, SECM has potential applications in biosensor research to study localized enzymatic activity over transducer surfaces independent of the transducer itself. It also allows the imaging of relative positions of active spots of immobilized enzymes. Furthermore, SECM is also efficiently used for the imaging of enzymatic activity over protein-tagged DNA or protein microarrays or chips. Although, SECM has been used as a tool in biosensor studies for a long time,[7] most of the studies on SECM imaging in biosensing studies were limited to rather large enzyme spots with microscale resolution.

Lately, there has been a tremendous increase in the use of nanomaterials for bioelectrochemical applications for developing new nanoscale sensing devices for future biological, medical, and electronic applications.[8–10] The reasons for such an increase are the high surface to volume ratio provided by nanomaterials over the transducer surface (that results in higher sensitivity and lower detection limit), their fast electron transfer efficiency and their specific electronic and optical properties. Among nanomaterials, nanotubes and nanowires

[a]*Institute of Analytical Chemistry, Chemo- and Biosensors, University of Regensburg, 93053 Regensburg, Germany. E-mail: frank-michael.matysik@chemie.uni-regensburg.de; Fax: +49-941-943-4491; Tel: +49-941-943-4548*

[b]*Division of Chemistry and Biological Chemistry, School of Physical Mathematical Sciences, Nanyang Technological University, 637371, Singapore*

† Dedicated to the memory of Prof. Craig Lunte.

‡ Electronic supplementary information (ESI) available. See DOI: 10.1039/c6ay01875k

are extensively used for sensor applications.[11–13] They are also termed as one dimensional (1-D) nanostructures because of a high ratio of their length (μm) to their diameter (nm). Gold nanowires (AuNWs) are fast gaining ground in sensing applications due to their high chemical and thermal stability, biocompatibility and excellent electrical conductivity.[14–24] Their ease of self-assembly over thiol modified transducer surfaces provides a stable matrix for electrochemical studies and/or for biomolecule assembly *via* chemical cross-linking. The recent trend towards the miniaturization of sensing devices encourages the use of single AuNWs for electrochemical studies.[25,26] Thus, it would be interesting to carry out SECM studies of individual AuNWs and to utilize its potential to map enzymatic activity distribution over them. Some of the recent publications have already established the role of SECM in the imaging and characterization of the electrochemical activity of individual nanomaterials.[27–29] Unwin and coworkers have extensively used scanning electrochemical cell microscopy (SECCM) to study individual biased single walled carbon nanotubes (SWCNTs) and their catalytic activity.[30,31] However, SECCM is not yet explored for electrochemical studies of unbiased individual nanomaterials. Besides, the immobilization and imaging of redox proteins over individual nanomaterials have not been reported so far. The classical constant height mode of SECM can be reliably used to image individual nanomaterials topographically and to study redox (enzymatic) activity over them. The distribution and stability of enzymatic activity (after immobilization) over an individual nanostructure can also be visualized *via* this technique.

In this work, we used SECM to image individual AuNWs over glass and gold-coated glass slides with high resolution using Wollaston-based Pt nanoprobes. The work was further extended by imaging the enzymatic peroxidase activity over individual AuNWs using ferrocenemethanol as the mediator system. The enzyme horseradish peroxidase (HRP) was used as the model enzyme for peroxidase activity imaging, as in addition to having an extensive biosensor potential, it is a commonly used tagging enzyme (enzyme label) for antibody or ligand molecules for molecular recognition or signal amplification in immunoassays, protein microarrays and SECM imaging studies.[17,23,32–34]

2. Materials and methods

2.1. Reagents

For all the SECM experiments, an aqueous solution of 1.5 mM ferrocenemethanol (99%, ABCR, Karlsruhe, Germany) containing 0.25 M KNO_3 as the supporting electrolyte was used as the mediator solution. The reagents (3-mercaptopropyl)triethoxysilane (MPTES), 1,4-butanedithiol, 11-mercaptoundecanoic acid, and *N*-hydroxysuccinimide (NHS) were obtained from Aldrich, Steinheim, Germany. *N*-(3-Dimethylaminopropyl)-*N*′-ethylcarbodimide hydrochloride (EDC) was obtained from Fluka, Steinheim, Germany. The enzyme horseradish peroxidase (HRP) was obtained from Serva GMBH, Germany. All other chemicals were of analytical reagent grade. The solutions were prepared in ultrapure water with a resistivity greater than 18 MΩ cm (membraPure, Bodenheim, Germany).

2.2. Fabrication of SECM probe electrodes

Sub-micrometer Pt disk UMEs (radii 500 nm and 300 nm) were prepared by using Wollaston-based Pt wires, whereas, the UMEs of larger radii (1–3 μm) were fabricated by using etched 25 μm diameter platinum wires, both obtained from Goodfellow, UK. The Wollaston-based Pt disk UMEs were fabricated according to the procedure described by Bond *et al.*[35] with partial modification. Briefly, the silver coated Pt wire was soldered to a copper lead. The wire was then inserted into a glass capillary (1.1–1.2 mm diameter) in such a way that the Wollaston wire protruded outside the capillary. The silver coating was then dissolved in concentrated nitric acid by dipping the tip of the wire in a drop of nitric acid with the help of a micromanipulator for ~30 min. The exposed Pt wire was then washed thoroughly in acetone and water to remove any debris on the wire. The wire was then retrieved inside the glass capillary and dried at 100 °C for 1 h to remove moisture. The Pt wire was then sealed inside the glass capillary (through the joint from where it was exposed from the silver coating) following the procedure described by Bergner *et al.*[36] A Kanthal wire (20 cm, 0.4 mm) was coiled in 10 loops and was heated by a DC power supply (~10 V) for 5–10 s. The capillary containing the exposed Pt wire was placed inside the loop until the sealing was complete. The probe was then inspected under a light microscope (100-fold magnification) to ensure that the exposed Pt wire did not break inside the glass capillary during heating and cooling of the glass around it. The disk shaped Pt electrode was then exposed by polishing with alumina polishing foils of decreasing grain sizes (30, 10, 3, 0.3, and 0.1 μm). Consecutively, a conically sharpened glass tip was prepared under a microscope with 500–1000 fold magnification (Keyence, Germany) by manually polishing the glass sealing from the sides with 0.3–0.1 μm alumina polishing foils. The etched Pt UMEs were fabricated by following the procedure described elsewhere.[2] The fabricated UMEs were characterized by steady state cyclic voltammetry and probe approach curves (PACs) using ferrocenemethanol as the mediator. A standard substrate (interdigitated electrodes produced by Micrux Technologies with 3 μm Pt strips separated by a 2 μm distance) was used to check the performance of the fabricated sub-micrometer probes in the feedback mode.

2.3. Synthesis of gold nanowires and their immobilization on substrates

Gold nanowires (AuNWs) were synthesized by the electrodeposition of gold on a polycarbonate membrane template by a modification of the procedure described by Mayorga-Martinez *et al.*[24] Prior to AuNW synthesis, an ultrathin gold-film was first sputtered on one side of a 0.1 μm isopore polycarbonate membrane (Merck Millipore) by using a conventional ion sputtering method to make the template conductive to be used as the working electrode. The membrane was then assembled in a plating cell by using an aluminum foil as contact. An Ag/AgCl electrode (CH Instruments, Austin, USA) and a 0.3 mm diameter platinum wire were used as the reference and counter electrodes, respectively. Gold was electrodeposited at −0.9 V for 60 s from a commercial plating solution (AMI DODUCO, Spain).

After electroplating, the sputtered gold layer was removed mechanically with a 3–4 μm alumina slurry. To release the nanowire from the polycarbonate template, the membrane was dissolved by immersing it in methylene chloride solution for 10 min. Finally, the solution was centrifuged at 6000 rpm for 2 min to pellet the nanowires. The pellet was then washed repeatedly with methylene chloride and ethanol with intermittent centrifugation and dissolution. The synthesized AuNWs were then inspected by TEM (JEOL Ltd., Japan).

AuNWs were immobilized on thiol-modified glass and gold-coated glass slides. The microscopic glass slide was cleaned overnight in concentrated nitric acid. The cleaned glass slide was rinsed with water, followed by drying with nitrogen gas and kept at 110 °C in an oven for 1 h. The oven dried slide was immediately immersed in a 5% solution of MPTES in anhydrous toluene for 30 min. After rinsing the thiosilane-modified glass slide with toluene and acetone several times, it was then dried at 110 °C in an oven for 1 h prior to use. The gold-coated glass slide (commercial surface plasmon resonance slide with a 50 nm thin film of gold) was thoroughly cleaned with ethanol and dried with nitrogen gas. A 10 mM ethanolic solution of 1,4-butanedithiol was drop-coated on the slide and left overnight. The dithiol modified slide was rinsed thoroughly with water before use.

An ethanolic solution of AuNWs was drop-coated on thiol-modified glass and gold-coated glass slides and left for ~6 h. The slides with immobilized AuNWs were rinsed thoroughly with water prior to SECM imaging to remove any unbound AuNWs. AuNWs were imaged electrochemically in the constant height mode at 0.3 V probe potential in ferrocenemethanol mediator solution.

Covalent-linking of HRP with AuNWs was achieved by partial modification of the procedure described by Saxena *et al.*[37] Briefly, 0.5 mM freshly prepared ethanolic solution of 11-mercaptoundecanoic acid was added to AuNWs in an Eppendorf cup and left for 5 h to obtain carboxylic group functionalized AuNWs. The solution was then centrifuged at 10 000 × *g* for 5 min to pellet AuNWs. The pellet was then washed with ethanol to remove unbound 11-mercaptoundecanoic acid. The carboxyl functionalized AuNWs were then treated with a solution of EDC (10 mg ml^{-1}) and NHS (50 mg ml^{-1}) for 10 min to activate the carboxylic groups on the AuNWs. Freshly prepared HRP solution (10 mg ml^{-1}) in sodium phosphate buffer (SPB, 50 mM, pH 6) was added to the above solution and kept at 4 °C for 12 h to obtain HRP-linked AuNWs. The HRP-linked AuNWs were then immobilized on the thiol modified gold-coated glass slide for subsequent feedback and peroxidase activity imaging by SECM. The localized HRP activity on AuNWs was imaged in the constant height mode by adding 0.3% H_2O_2 to the ferrocenemethanol solution and applying a probe potential of 0 V. The ferrocenemethanol solution for activity imaging was prepared in SPB.

2.4. Electrochemical and AFM instrumentation

A commercial SECM system CHI 920c (CH Instruments, Austin, USA) was used for all experiments. It consisted of a bipotentiostat and a motor control unit that controls both the stepper motor and the piezo positioner. A tailor-made electrochemical cell (Teflon) with two clamps (polyether ether ketone, PEEK) and four integrated screws (Teflon) for substrate fixation was used. The electrochemical cell was bolted on a stainless steel carrier that was levelled using three micrometer adjustment screws. A Pt electrode was used both as the reference and counter electrodes throughout the SECM experiments. All the potentials mentioned in this paper refer to this quasi-reference electrode.

AFM imaging of all the AuNW modified substrates was performed with a commercial system nanosurf easyScan 2 (Nanoscience Instruments, Phoenix, USA) and AFM probes PPP-NCLR (Nanoscience Instruments, Phoenix, USA) in the tapping mode.

3. Results and discussion

3.1. Probe electrode fabrication and characterization

Wollaston-based Pt UMEs have been used for a long time for electrochemical studies[35] and SECM imaging.[2] However, the fabrication of sub-micrometer UME probes was always a challenge because of the fragility of the exposed Pt nanowires and the difficulty of sealing them inside glass capillaries which required a lot of practice and patience. Despite these limitations, the robustness of Wollaston-based Pt UMEs makes them an interesting target for exploitation in SECM imaging studies. With some minor modifications (as discussed in the Experimental section before) in the already established fabrication protocol of Wollaston-based Pt UMEs, we were able to fabricate probes down to radii of 300 nm on a regular basis. The probes once sealed and polished were robust enough to be used for multiple scans over long periods of time with intermittent cleaning and polishing. Thus, Wollaston-based probes provided an advantage over other relatively fragile sub-micrometer Pt disk probes fabricated by alternative methods such as Pt wire etching or capillary pulling. Fig. 1A shows the cyclic voltammograms of the sub-micrometer Wollaston-based Pt UMEs. Well-defined voltammograms with minor hysteresis and stable steady state currents were obtained. With cone formation, a RG value of ~10 was achieved for a 500 nm radius probe, whereas, the RG for a 300 nm radius probe was more than 10 (Fig. S1, ESI‡). The probe approach curves over a flat glass substrate and a gold-coated glass substrate were recorded for the calculation of the RG of the fabricated 300 nm radius Wollaston-based Pt UME (Fig. S2, ESI‡). A high resolution image of an interdigitated Micrux electrode with 3 μm Pt strips separated by a 2 μm distance (non-conductive Pyrex material) was recorded with a 300 nm radius UME (Fig. 1B). A strong positive feedback current (~200 pA) because of the recycling of ferrocenemethanol at the Pt surface was recorded which was well resolved from the negative feedback current (~70 pA) from the Pyrex material in between the Pt strips. The I_0 was ~100 pA. The SECM image of the interdigitated electrode structure correlated very well with its AFM image (Fig. 1B inset). The flat surfaces of Pt strips as recorded in the AFM image were also visible in the corresponding SECM image. Fig. S3 (ESI‡) shows the representative areas imaged by SECM and AFM. The apparent width of the

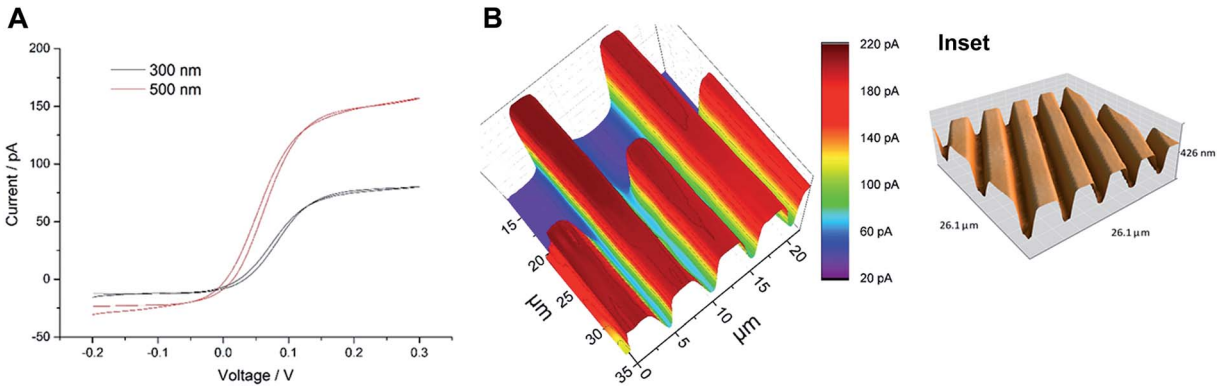

Fig. 1 (A) Cyclic voltammograms of Wollaston-based Pt UMEs of different radii (500 nm and 300 nm) at a scan rate of 50 mV s^{-1}. (B) High-resolution SECM image of an interdigitated Micrux electrode with 3 µm Pt strips separated by a 2 µm distance (non-conductive Pyrex material). The image was recorded with a 300 nm radius Pt probe at a potential of 0.3 V and a scan rate of 12.5 µm s^{-1} in 1.5 mM ferrocenemethanol solution (inset: representative AFM image of the same substrate; for detailed insight, see Fig. S3, ESI‡).

unbiased conductive Pt strip in the SECM image correlated closely with the actual width of the strip. Thus, the 300 nm radius probe was considered to be potentially suitable to image AuNWs which were 2–3 µm long and ~140 nm in diameter.

3.2. Feedback imaging of AuNWs

The characterization of the synthesized AuNWs with TEM showed that the average AuNWs were 2–3 µm long and ~140 nm in diameter (Fig. S4, ESI‡). Later, an approach for the immobilization of AuNWs on a thiosilane-modified glass slide was developed. The nanowires immobilized on the glass substrate were stable for frequent SECM scans in mediator solution. The AuNWs on glass slides did not show a positive feedback current response by mediator recycling despite being a conductor. Instead, negative topographic images were recorded for individual AuNWs by using a 300 nm radius probe within 70–80% I_0 (Fig. 2A). Fig. 2B shows a representative AFM image of immobilized AuNWs on a glass slide. The negative feedback image of individual AuNWs immobilized on an insulating glass surface was intriguing and the reason could be attributed to their inability to act as efficient bipolar substrates (enabling an anodic reaction at some distance from the cathodic mediator regeneration at the unbiased AuNWs in the probe vicinity). Normally, when a conducting substrate has a smaller area compared to that of the probe, positive feedback is significantly limited by the substrate's ability to act as an efficient bipolar electrode and the substrate could get charged with time. However, in one of the recent reports by Oleinick *et al.*,[38] it has been shown experimentally that if the substrate extends beyond the area covered by the tip, the constraints due to the bipolar function become negligible because the extended parts of the conductor may act as an efficient second pole of the bipolar substrate exchanging electrons with the bulk solution. In our experiment, the diameter of the AuNW (~140 nm) was significantly smaller than the Pt probe diameter (600 nm). However, the relatively extended length of the nanowire (2–3 µm) was still not sufficient for effective recycling of the electrons with the bulk mediator solution resulting in a negative feedback current response. Previously, Amemiya and co-workers[27,28] were able to record positive feedback images of lithographically cast gold nanobands (100 nm broad and 50 µm long) and single walled carbon nanotubes (~1.6 nm diameter and ~2 mm long) on insulating surfaces with probes of diameters ~2 µm and 10 µm, respectively. Although, the diameters of probes used to record these images were rather large compared to those of the ones used in our studies with AuNWs, the extremely extended lengths of these bands and nanowires were sufficient to exchange electrons with the bulk solution and to behave as bipolar substrates. Thus, a certain minimum ratio of length of the nanowire to the Pt tip diameter was necessary to have an effective second pole, which could exchange electrons with the bulk solution and facilitate a positive feedback response from the unbiased AuNWs. Additionally, a significantly larger RG (between ~15–30) of the 300 nm radius probe could also have had a shielding effect for the flow of bulk mediator solution towards the far ends of individual AuNWs below the tip,

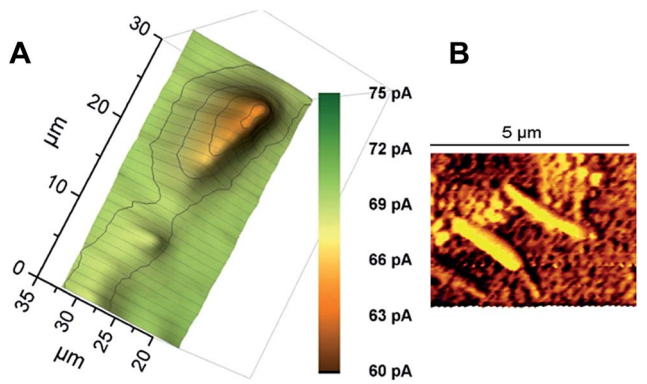

Fig. 2 (A) Negative feedback SECM image of individual AuNWs immobilized on a glass slide. The image was recorded with a 300 nm radius Pt probe at a potential of 0.3 V and a scan rate of 5 µm s^{-1} in 1.5 mM ferrocenemethanol solution. (B) Representative AFM image of AuNWs immobilized on a glass slide.

hindering the exchange of electrons from them. A similar effect of RG was observed by Xiong *et al.*,[39] where the positive feedback from an unbiased conducting substrate was found to depend on the thickness of the insulating layer surrounding the metal disk probe of comparable radius, which hindered mediator diffusion from the bulk solution to the substrate. However, they also showed that the current approach curves changed from negative to positive as RG was changed from 50 to 1.1. Although, the length of 1-D nanostructures compared to the probe diameters (including RG) is well known to have an effect on the feedback response (negative or positive) from the unbiased conducting substrates,[27,39] a clear negative feedback current image of an individual unbiased conducting nanowire immobilized over an insulating substrate has not been reported before.

To further investigate the above observation, AuNWs were immobilized on a glass slide coated with a thin film of gold. A well-dispersed assembly of AuNWs over the thiol-modified gold-coated glass slide was achieved as seen in the representative AFM images (Fig. 3C and D). The AuNWs immobilized on the gold-coated slide were stable enough to be scanned frequently by using SECM probes. Positive feedback approach curves over an entire thiol-modified gold surface were recorded which showed that thiol-modification did not interfere with the recycling of the mediator over the bulk gold surface. Well-resolved positive feedback images of both clustered as well as individual AuNWs were recorded with a 300 nm radius probe within 105–110% I_0 over the conducting gold surface (Fig. 3A and B). The extended conducting surface (thin conducting gold film in this case) beyond the tip area facilitated the recycling of electrons of nanowires with the bulk mediator solution resulting in a positive feedback response. The visibly differentiated contrast of AuNWs over a bulk gold surface was the result of the differences in topography (effectively exposed surface area for recycling of the mediator) and in intrinsic conductivity of the AuNWs and thin-film gold surface. However, the positive feedback on the AuNWs supported the fact that the immobilized AuNWs were effectively electrically connected with the bulk gold surface. This result supports the fact that SECM can be used as a method of choice for the characterization of immobilization of nanomaterials as a support matrix for biomolecule assembly over transducer surfaces in addition to other physical and electrochemical methods.

An apparent width of ~10 μm with ~5 pA of negative feedback current was recorded for individual AuNWs immobilized on a glass slide (Fig. 4A). On the other hand, an apparent width of ~1.5–2 μm with ~2 pA positive feedback current was recorded for individual AuNWs immobilized on a gold-coated glass slide (Fig. 4B). The apparent width of the nanowire in the negative feedback image was largely affected by the big RG of the probe, whereas in the positive feedback image over the bulk gold substrate, it was almost independent of the RG. When compared to negative feedback current, a smaller difference in positive feedback current over individual AuNWs from the bulk substrate was recorded because of the positive background current contributed by the bulk gold film. The differences in overall current between negative and positive feedback current images (Fig. 2A and 3B) and even between different positive feedback current images of individual AuNWs (Fig. 3B and 7A) were due to different batches of mediator solutions and sometimes due to partial fouling of the probes used.

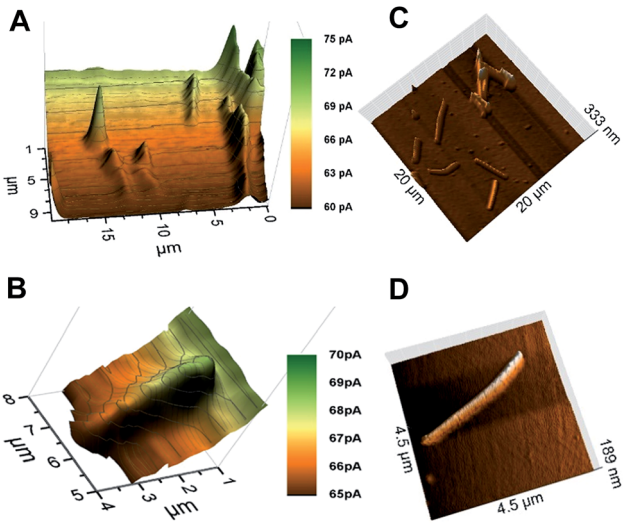

Fig. 3 (A and B) Positive feedback SECM images of clustered and individual AuNWs immobilized on a gold-coated glass slide. The image was recorded with a 300 nm radius Pt probe at a potential of 0.3 V and a scan rate of 5 μm s^{-1} in 1.5 mM ferrocenemethanol solution. (C and D) Representative AFM images of AuNWs immobilized on a gold-coated glass slide.

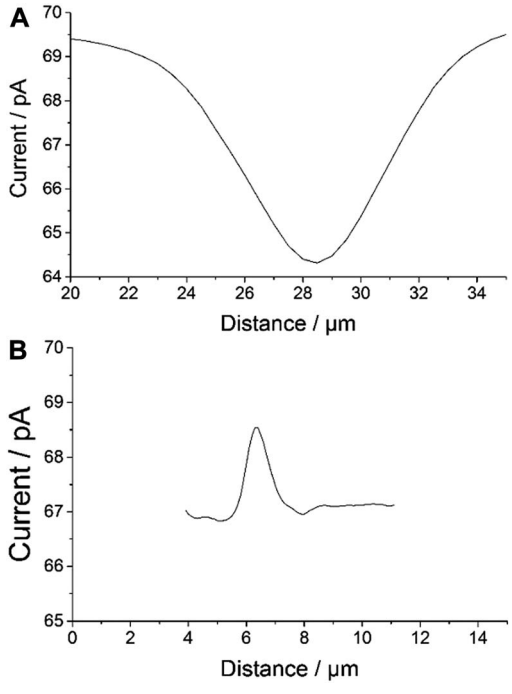

Fig. 4 SECM line scans across individual AuNWs with (A) negative (over glass slide) and (B) positive (over gold-coated glass slide) feedback current responses. The line scans were obtained with a 300 nm radius Pt probe at a potential of 0.3 V in 1.5 mM ferrocenemethanol solution.

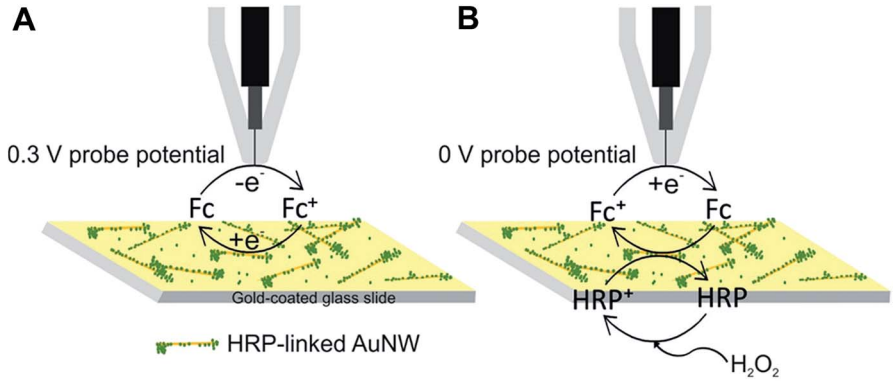

Fig. 5 Schematic representation of (A) positive feedback at 0.3 V probe potential and (B) SG/TC at 0 V probe potential over HRP-linked AuNWs in ferrocenemethanol solution (diagram not to scale).

Although, the apparent width of the AuNW in the positive feedback image was almost independent of the RG of the tip, it was largely dependent on the Pt disk diameter. The AuNW appeared wider than its actual diameter (Fig. 3B and 4B), whereas, the apparent length of the nanowire was similar to its actual length as seen in the representative AFM image (Fig. 3D). Since the apparent dimensions of the nanostructures in high-resolution SECM are largely dependent on the probe diameters, the nanostructures appeared even broader in the earlier reports by Amemiya and co-workers,[27,28] where they used relatively larger diameter probes to image the gold nanoband and carbon nanotube. However, the broadening of the carbon nanotube was significantly decreased when scanned across with a 1.5 μm diameter Pt probe. The apparent width of the nanotube was around 4 times the diameter of the Pt disk.[28] The observation correlated closely with our studies with a 300 nm radius probe, where the apparent width in the positive feedback image was around 3 times the diameter of the Pt disk. The recent publications by Mirkin and co-workers have reported the imaging and catalytic efficiency of individual gold nanoparticles (AuNPs, 10–20 nm diameter) with an extremely small probe of radius ≥3 nm.[29,40] Although, they could record a positive feedback current over individual AuNPs with a probe of radius 42 nm (where the AuNPs were electrically connected *via* an underlying highly ordered pyrolytic graphite surface), the image resolution impressively improved with decreasing probe sizes. With the probes of radii 14 nm and 3 nm, the SECM measurements quite close to actual diameters were made for 20 nm and 10 nm diameter AuNPs, respectively.

Although, a closer correlation of apparent and actual nano-dimensions could be achieved in SECM images with decreasing probe sizes, the Wollaston-based 300 nm radius Pt probe appeared to be an appropriate choice to image immobilized AuNWs in our case. As seen in the representative AFM images (Fig. 3C and inset of Fig. 6), the assembly of AuNWs over the substrates was not even. Entangled AuNW bundles of various sizes were frequently encountered during the constant height scans of the substrates which could have easily destroyed the etched or capillary pulled nano-probes with smaller RGs. The probes used in our studies were robust enough to be used again after crashing into these bundles with intermittent cleaning and polishing.

Since the apparent dimensions of individual AuNWs immobilized on gold-coated glass slides correlated better with the actual dimensions, the same was chosen for enzyme (HRP) activity imaging studies.

3.3. Subsequent feedback and activity imaging of HRP-linked AuNWs

For imaging of peroxidase activity, HRP was covalently linked to AuNWs by the EDC-NHS method. The HRP-linked AuNWs were then immobilized on the gold-coated glass slide. Generally, the catalytic cycle of HRP involves the reaction of a ferric form of the

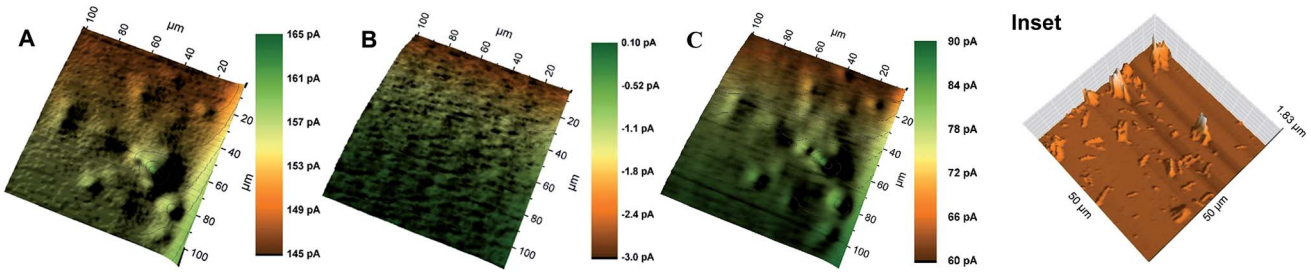

Fig. 6 SECM images of HRP-linked AuNW clusters immobilized on a gold-coated glass slide at (A) 0.3 V probe potential (positive feedback), (B) 0 V probe potential, and (C) 0 V probe potential after the addition of 0.3% H_2O_2 (SG/TC). The images were recorded with Pt probes of radii 1–3 μm at a scan rate of 50 μm s^{-1} in 1.5 mM ferrocenemethanol solution in pH 6 SPB. Inset: representative AFM image of the same substrate.

protein (Fe^{III}) with H_2O_2 to give the ferryloxy radical (Fe^{IV}=O) of the enzyme known as compound I. The ferryloxy radical reacts with an electron donor to give the non-radical ferryloxy form (Fe^{IV}=O) of the enzyme known as compound II which then reacts with H_2O_2 to give an oxyperoxidase form of the enzyme that decomposes to superoxide and Fe^{III}. The resulting HRP activity could either be imaged by recording the peroxide consumption at high overpotential (~1 V)[41] or by imaging the reduction of the electron donor oxidized by HRP. Ferrocenemethanol was used as an electron donor for HRP in this work which was then reduced at the Pt probe at a potential of 0 V. A similar mechanism was used previously for SECM imaging of HRP-labelled protein microarrays.[33] As shown in Fig. 5, at 0.3 V probe potential, the AuNWs were imaged in the feedback mode, whereas by switching the probe potential to 0 V after the addition of H_2O_2, the peroxidase activity of HRP covalently linked to AuNWs can be imaged subsequently in the same experiment. Fig. 6A shows the positive feedback image of ferrocenemethanol recycling at AuNW clusters (representative AFM image, inset of Fig. 6) at a probe potential of 0.3 V. When the potential was switched to 0 V, no current was recorded at the probe (Fig. 6B). However, when H_2O_2 was added to the same mediator solution, HRP activity was imaged at AuNW clusters by the reduction of HRP oxidized ferrocenemethanol at a Pt UME in the substrate generation/tip collection (SG/TC) mode (Fig. 6C). Interestingly, although the measured current in the SG/TC imaging of AuNW clusters was nearly half of the measured current in the positive feedback image, a current difference of ~30 pA was recorded over the AuNW clusters from the bulk substrate in the SG/TC mode. This difference was significantly higher than the current difference (~20 pA) recorded in the positive feedback mode. The observation suggests the localization of HRP activity over and around AuNW clusters rather than on the bulk substrate surface resulting in less background current in the SG/TC mode at 0 V. This also confirms the stable covalent linking of HRP with the AuNWs. In the positive feedback image at 0.3 V, the bulk gold substrate surface contributed towards a higher background current, and thus resulted in a lower current difference over AuNWs. However, a considerably higher positive feedback response from the AuNWs from the bulk gold substrate further supported our above observation that covalent-linking of HRP with the carboxyl groups of the thiol-modified AuNWs did not interfere with the recycling of the ferrocenemethanol mediator at 0.3 V probe potential (Fig. 6A). The same was also observed by an unhindered positive feedback response from individual AuNWs (HRP-modified) at 0.3 V probe potential in Fig. 7A.

Some of the recent research studies focused on the use of a single AuNW or AuNP to study catalytic properties and sensing,[25–29,37,38] which prompted us to image the distribution of HRP activity over individual AuNWs. Fig. 7A and B show the images of individual AuNWs in the feedback and SG/TC modes at 0.3 V and 0 V (in the presence of H_2O_2) probe potentials, respectively. Interestingly, although the HRP activity was distributed along the entire length of AuNWs, higher enzymatic activity was imaged at the ends of nanowires. The representative AFM image of the HRP-linked AuNWs (Fig. 7C) shows that HRP

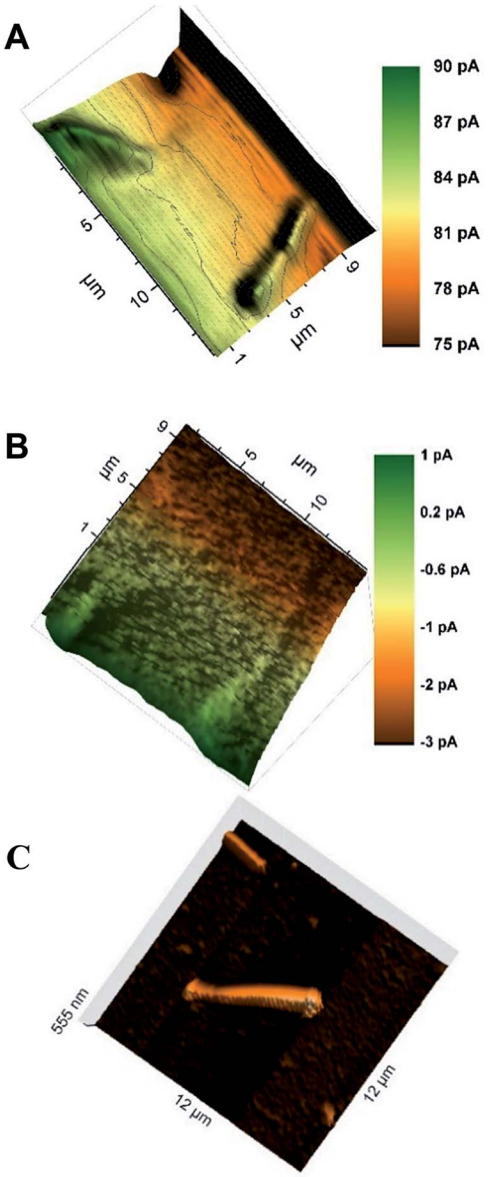

Fig. 7 SECM images of individual HRP-linked AuNWs immobilized on a gold-coated glass slide at (A) 0.3 V probe potential (positive feedback) and (B) 0 V probe potential after the addition of 0.3% H_2O_2 (SG/TC). The images were recorded with a 300 nm radius probe at a scan rate of 5 μm s^{-1} in 1.5 mM ferrocenemethanol solution in pH 6 SPB. (C) Representative AFM image of the same substrate.

was immobilized throughout the length of the nanowires. However, the ends of AuNWs showed relatively larger aggregation of immobilized HRP which correlated well with the corresponding SECM image.

Since the current recorded at individual AuNWs in the SG/TC mode was very small (~2 pA), a clear image from the background current could not be differentiated; so, a comparison with positive feedback current cannot be made. A drift in current along the length of the wire was observed mainly due to a slight tilt in the substrate. Since the measured enzymatic activity in the SG/TC mode was small, the drift appears quite pronounced in the image. A similar drift (but

not so pronounced) was also observed in the corresponding positive feedback image of AuNWs. This is one of the first reports (to the best of our knowledge), where SECM imaging of enzymatic activity at individual nanomaterials was achieved. A similar amount of current (~2 pA) was mapped at around 1 V probe potential over individual AuNPs (~200 nm diameter) with a bias potential of 0.4 V by Wain's research group.[41] Thus, a similar current over unbiased HRP-linked AuNWs at 0 V probe potential provides a more feasible alternative for signal mapping over various DNA or protein microarrays.

4. Conclusions

Subsequent feedback and enzymatic peroxidase activity over individual AuNWs were imaged using a 300 nm radius Wollaston-based Pt probe in the constant height mode of SECM. The SECM imaging of enzymatic activity at individual nanomaterials is reported for the first time. The observations could be extended to study the catalytic properties of other nanomaterials or to characterize enzyme modified electrode surfaces (biased or unbiased) or to map amplified signals over HRP-linked DNA or protein microarrays with sub-micrometer resolutions. The negative and positive feedback responses of individual AuNWs immobilized on insulating and conducting film surfaces, respectively, provided insight into the factors affecting the effective recycling of the mediator by conducting nanomaterials particularly by 1-D nanostructures. The imaging with a positive feedback current response of individual AuNWs (~140 nm wide) over a bulk conducting substrate using a rather large 300 nm radius Pt probe also eliminates the requirement for very small probes for imaging of unmodified or variously modified conductive nanomaterials. The work also establishes the importance of the constant height mode of SECM in surface characterization of transducers after nanomaterial/biomolecule immobilization in biosensing applications providing additional electrical connectivity/activity distribution data to the topographic details provided by other microscopy methods.

Acknowledgements

Dr Preety Vatsyayan is thankful to the Alexander von Humboldt Foundation for the postdoctoral fellowship. The authors also acknowledge the support from the Professor Merkoçi research group at the Catalan Institute of Nanotechnology, Barcelona, Spain, for the synthesis of gold nanowires.

References

1 A. J. Bard, F.-R. F. Fan, J. Kwak and O. Lev, *Anal. Chem.*, 1989, **61**, 132–138.
2 A. J. Bard, *Electroanal. Chem.*, Marcel Dekker, New York, 1994, vol. 18.
3 S. Bergner, P. Vatsyayan and F.-M. Matysik, *Anal. Chim. Acta*, 2013, **775**, 1–13.
4 S. Amemiya, A. J. Bard, F.-R. F. Fan, M. V. Mirkin and P. R. Unwin, *Annu. Rev. Anal. Chem.*, 2008, **1**, 95–131.
5 P. Sun, F. O. Laforge, T. P. Abeyweera, S. A. Rotenberg, J. Carpino and M. V. Mirkin, *Proc. Natl. Acad. Sci. U. S. A.*, 2008, **105**, 443–448.
6 F. O. Laforge, J. Velmurugan, Y. Wang and M. V. Mirkin, *Anal. Chem.*, 2009, **81**, 3143–3150.
7 L. Stoica, S. Neugebauer and W. Schuhmann, *Adv. Biochem. Eng./Biotechnol.*, 2008, **109**, 455–492.
8 M. Holzinger, A. Le Goff and S. Cosnier, *Front. Chem.*, 2014, **2**, 1–10.
9 P. Vatsyayan, in *Bioanal. Rev.*, ed. F. M. Matysik, Springer, Berlin Heidelberg, 2016, DOI: 10.1007/11663_2015_5001.
10 D. Battistel, F. Baldi, M. Gallo, C. Faleri and S. Daniele, *Talanta*, 2015, **132**, 294–300.
11 A. K. Wanekaya, W. Chen, N. V. Myung and A. Mulchandani, *Electroanalysis*, 2006, **18**, 533–550.
12 U. Yogeswaran and S.-M. Chen, *Sensors*, 2008, **8**, 290–313.
13 A. M. Kumar, S. Jung and T. Ji, *Sensors*, 2011, **11**, 5087–5111.
14 S. Cherevko and C.-H. Chung, *Sens. Actuators, B*, 2009, **142**, 216–223.
15 X. Zhang, D. Li, L. Bourgeois, H. Wang and P. A. Webley, *ChemPhysChem.*, 2009, **10**, 436–441.
16 M. Yang, F. Qu, Y. Li, Y. He, G. Shen and R. Yu, *Biosens. Bioelectron.*, 2007, **23**, 414–420.
17 J. Xu, F. Shang, J. H. T. Luong, K. M. Razeeb and J. D. Glennon, *Biosens. Bioelectron.*, 2010, **25**, 1313–1318.
18 Y. Lu, M. Yang, F. Qu, G. Shen and R. Yu, *Bioelectrochemistry*, 2007, **71**, 211–216.
19 S. Aravamudhan, A. Kumar, S. Mohapatra and S. Bhansali, *Biosens. Bioelectron.*, 2007, **22**, 2289–2294.
20 S. Aravamudhan, N. S. Ramgir and S. Bhansali, *Sens. Actuators, B*, 2007, **127**, 29–35.
21 A. Cusmà, A. Curulli, D. Zane, S. Kaciulis and G. Padeletti, *Mater. Sci. Eng., C*, 2007, **27**, 1158–1161.
22 S. Guo, D. Wen, S. Dong and E. Wang, *Talanta*, 2009, **77**, 1510–1517.
23 H. Zhong, R. Yuan, Y. Chai, W. Li, Y. Zhang and C. Wang, *Bioprocess Biosyst. Eng.*, 2011, **34**, 923–930.
24 C. C. Mayorga-Martinez, M. Guix, R. E. Madrid and A. Merkoci, *Chem. Commun.*, 2012, **48**, 1686–1688.
25 K. Dawson, M. Baudequin and A. O'Riordan, *Analyst*, 2011, **136**, 4507–4513.
26 K. Dawson, A. Wahl, R. Murphy and A. O'Riordan, *J. Phys. Chem. C*, 2012, **116**, 14665–14673.
27 H. Xiong, J. Kim, E. Kim and S. J. Amemiya, *J. Electroanal. Chem.*, 2009, **629**, 78–86.
28 J. Kim, H. Xiong, M. Hofmann, J. Kong and S. Amemiya, *Anal. Chem.*, 2010, **82**, 1605–1607.
29 T. Sun, Y. Yu, B. J. Zacher and M. V. Mirkin, *Angew. Chem., Int. Ed.*, 2014, **53**, 14120–14123.
30 A. G. Güell, K. E. Meadows, P. V. Dudin, N. Ebejer, J. V. Macpherson and P. R. Unwin, *Nano Lett.*, 2014, **14**, 220–224.
31 A. G. Güell, N. Ebejer, M. E. Snowden, K. McKelvey, J. V. Macpherson and P. R. Unwin, *Proc. Natl. Acad. Sci. U. S. A.*, 2012, **109**, 11487–11492.
32 H. Shiku, T. Matsue and I. Uchida, *Anal. Chem.*, 1996, **68**, 1276–1278.

33 T. Kai, S. Chen, E. Monterroso and F. Zhou, *Anal. Chem.*, 2015, **87**, 4523–4529.
34 E. Fortin, P. Mailley and L. L. S. Szunerits, *Analyst*, 2006, **131**, 186–193.
35 A. M. Bond, M. Fleischmann and J. J. Robinson, *Electroanal. Chem.*, 1984, **168**, 299–312.
36 S. Bergner, J. Wegener and F.-M. Matysik, *Anal. Chem.*, 2011, **83**, 169–174.
37 U. Saxena, M. Chakraborty and P. Goswami, *Biosens. Bioelectron.*, 2011, **26**, 3037–3043.
38 A. I. Oleinick, D. Battistel, S. Daniele, I. Svir and C. Amatore, *Anal. Chem.*, 2011, **83**, 4887–4893.
39 H. Xiong, J. Guo and S. Amemiya, *Anal. Chem.*, 2007, **79**, 2735–2744.
40 Y. Yu, T. Sun and M. V. Mirkin, *Anal. Chem.*, 2015, **87**, 7446–7453.
41 M. A. O'Connell, J. R. Lewis and A. J. Wain, *Chem. Commun.*, 2015, **51**, 10314–10317.